Single Live Cell Imaging of Chromosomes in Chloramphenicol-Induced Filamentous *Pseudomonas aeruginosa*†

Christina Steel, Qian Wan, and Xiao-Hong Nancy Xu*

Department of Chemistry and Biochemistry, Old Dominion University, Norfolk, Virginia 23529

Received July 29, 2003; Revised Manuscript Received October 9, 2003

ABSTRACT: *Pseudomonas aeruginosa* is a leading opportunistic pathogen in human infections, and it is renowned for its intrinsic resistance to structurally and functionally unrelated antibiotics. Filamentation induced by antibiotics appears to trigger bacteria to depart from a normal growth phase and enter a stationary growth phase. As antibiotic concentrations decline below a therapeutic range, filamentous bacteria begin to divide normally, leading to a more rapid regrowth of the bacteria. Furthermore, filamentous bacteria are associated with an increase in endotoxin release. Moreover, the immune system of a patient needs to cope with uncharacteristic filamentous bacteria. Thus, it is biologically and clinically significant to study and understand bacterial filamentation. In this study, we investigate the frequencies, conditions, and characteristics of a filamentous *P. aeruginosa* at single cell and single chromosome resolutions. Our results show that filamentous cells (elongated rods) contain multiple copies of the cell's chromosome. It appears that the unsuccessful segregation of replicated chromosomes in an individual cell accompanies the formation of undivided filamentous cells. The quantity of chromosomes and the length of the filamentous wild-type cells increase as the chloramphenicol concentration increases to 50 and 250 μg/mL, suggesting that chloramphenicol induces the filamentation. Filamentation in three strains of *P. aeruginosa* depends on the expression level of efflux pump (MexAB-OprM) and the minimum inhibitory concentration of chloramphenicol. This study also opens up the new possibility of real-time monitoring of modes of actions of antibiotics in live cells with both temporal and spatial resolution.

It has been reported previously that a variety of antibiotics induce filamentation in Gram-negative bacteria, and the majority of these studies employed β-lactam antibiotics (*1*−*8*). It is generally believed that β-lactam antibiotics induce bacterial filamentation by inhibiting penicillin-binding proteins (PBPs)[1] (*2*−*4*). Such inhibition terminates the assembly of the peptidoglycan network in the bacterial cell wall. Inhibition of PBP-1 leads to rapid cell death, whereas inhibition of PBP-2 and PBP-3 leads to changes in cell morphologies, turning normal cells to spheroplasts and filamentous cells (elongated rods), respectively (*2*−*3*). Normally, PBP-3 catalyzes the formation of the septum in dividing bacteria, and the mechanism of such actions involves a transpeptidase (*4*). Thus, inhibition of this protein (PBP-3) leads to the incomplete formation or absence of septa in dividing bacteria, resulting in the formation of long strands of bacteria (filaments). In addition, filamentation induced by antibiotics appears to trigger the cells to depart from a normal growth phase and enter a stationary growth phase. As antibiotic concentrations decline below a therapeutic range, filamentous bacteria begin to divide normally and produce normal sized cells, leading to a more rapid regrowth of the bacteria due to a swift increase in the number of available colony-forming units (CFU) (*4*). Furthermore, filamentous bacteria are associated with an increase in endotoxin (lipopolysaccharide, LPS) release (*3*). LPS is a biological and clinical important compound, creating a wide spectrum of physiological reactions including changes in white blood cell counts, tumor necrosis, and dissemination of intravascular coagulation. A high concentration of free LPS in solution is lethal to humans. Moreover, the immune system of patients needs to cope with these uncharacteristic forms (filament) of bacteria (*9*). Therefore, it is biologically and clinically significant to study and understand bacterial filamentation.

Previous studies of filamentation have focused primarily on the changes in cellular morphology as normal cells turn to filamentous cells using electron microscopy (*2*, *5*, *7*, *8*, *10*−*12*), X-ray micrography (*6*), and phase-contrast optical microscopy (*5*, *10*). However, these techniques are used to image the morphology of the dead cells, and temporal information on how antibiotics affect the replication of chromosomes in live cells cannot be obtained. Recently, the fluorescent staining assays (e.g., DAPI imaging) have become a popular tool for the study of chromosomes (*13*). Unfortunately, the fluorescent staining assays are quite often applied with cell fixation and a high concentration of fluorescent dyes, frequently resulting in cell death. Consequently, the fluorescent staining assays are unable to offer real-time temporal information on the mechanism(s) of filamentation and the modes of action of antibiotics in live cells. Thus,

† This work was supported in part by NIH (RR15057-01), Old Dominion University, in the form of a start-up fund, and a Dominion Scholar Fellowship (Q.W.).

* To whom correspondence should be addressed. E-mail: xhxu@odu.edu. Tel/fax: (757) 683-5698.

[1] Abbreviations: ADC, analog and digital count; CFU, colony-forming units; DAPI, 6′-diamidino-2-phenylindole hydrochloride; EtBr, ethidium bromide; PBP, penicillin binding protein; LPS, lipopolysaccharide; MIC, minimum inhibitory concentration; MDR, multidrug resistance; *P. aeruginosa*, *Pseudomonas aeruginosa*; WT, wild-type.

10.1021/bi035341e CCC: $27.50
Published on Web 12/10/2003

the mechanism of bacterial filamentation remains incompletely understood.

Unlike the previous studies, we use single live cell imaging to characterize filamentous bacteria, directly observing replication of chromosomes in individual cells, and to investigate the role of chromosomes in filamentation. In this study, *Pseudomonas aeruginosa* is selected because it is a ubiquitous Gram-negative bacterium and is a leading cause of nosocomial infections in cancer, transplant, burn, and cystic fibrosis patients (*14*−*16*). These infections are impossible to eradicate due in part to the resistance of *P. aeruginosa* to multiple classes of antibiotics (*14*−*16*), which is attributable to several efflux pumps in *P. aeruginosa*, including MexAB-OprM, MexCD-OprJ, MexEF-OprN, and MexXY-OprM (*17*, *18*). The MexAB-OprM is the major efflux pump in wild-type (WT) cells. This pump consists of two inner membrane proteins (MexA and MexB) and one outer membrane proteins (OprM) (*17*, *18*). Despite extensive research over decades, the extrusion mechanism in bacteria still remains essentially unknown (*14*−*16*). In this study, three strains of *P. aeruginosa* (WT, nalB-1, and ΔABM) (*19*−*21*) are used to determine the characteristics of filaments associated with the different expression levels of the extrusion pump (MexAB-OprM). Studying the mechanisms of filamentation of mutants will lead to a better understanding of the role of multidrug resistance (MDR) in the formation of filamentous cells.

In this study, ethidium bromide (EtBr) is used as a fluorescent probe to study chromosomes in chloramphenicol-induced filamentous *P. aeruginosa* using our real-time live cell imaging. EtBr has been widely used as a fluorescence probe to study the uptake and extrusion mechanism in *P. aeruginosa* (*16*, *19*, *22*−*28*). It is well-known that EtBr passively diffuses through the membrane of *P. aeruginosa* and can be extruded out of cells by an efflux pump, preventing an overdose of EtBr from being accumulated in the cells (*16*, *19*, *22*). Furthermore, the minimum inhibitory concentration (MIC) of EtBr for *P. aeruginosa* is higher than 1 mM (*19*, *26*). Thus, the cells can still be alive while high concentrations of EtBr are accumulated in live cells. EtBr emits a weaker fluorescence emission in aqueous environments and becomes strongly fluorescent in nonpolar or hydrophobic environments. The quantum yield of EtBr intercalated with DNA is about 10 times higher than that of EtBr in buffer solution (*22*), allowing a single copy of chromosomes in live bacterial cells to be directly observed.

In this study, we investigate the filamentation of *P. aeruginosa* in response to the change of chloramphenicol concentration, aiming to determine the condition and frequency of filamentation and to understand the size distribution of filaments associated with the amount and distribution of their chromosomes. Such studies can enhance our understanding of the conditions leading to bacterial filamentation and its mechanism. A better understanding of bacterial filamentous cells will lead to the improved treatment of severe bacterial infections using antibiotics.

MATERIALS AND METHODS

Reagents and Cell Strains. Chloramphenicol solutions were prepared by dissolving chloramphenicol in 95% ethanol (25 mg/mL) and diluting the solution to 2.5 mg/mL using autoclaved ultrapure water (Nanopore, ≥18 MΩ sterilized) (*29*−*32*). EtBr solution prepared using ultrapure water was triple filtered using 0.22 μm membrane filters (sterilized, Costar). All chemicals were purchased from Sigma and were used directly without further purification.

Three strains of *P. aeruginosa*, WT (PAO4290, a strain that expresses the same level of MexAB-OprM as a wide type), nalB-1 (TNP030#1, a mutant strain that overexpresses MexAB-OprM), and ΔABM (TNP076, a mutant devoid of MexAB-OprM), were used (*19*−*21*). The cells were prepared in a 2 mL of L-broth (1% tryptone peptone, 0.5% yeast extract, 0.5% NaCl, pH 7.2) and incubated in a shaker (Lab-Line Orbit Envivon-shaker) at 37 °C and 120 rpm for 21 h to ensure a full growth. Cells were then cultured in 3 mL of L-broth containing 300 μL of precultured cells and chloramphenicol concentrations of 0, 6.25, 12.5, 25.0, 50.0, and 250 μg/mL, respectively. Such cell suspensions were incubated in the shaker at 37 °C and 120 rpm for 9 h to prepare cultured cells. Another 3 mL of solution containing 10 μM EtBr and 150 μL of the cultured cells was prepared and incubated at 37 °C for an additional 2 h before taking absorbance measurements at 600 nm and dark-field microscopic images. To determine the proliferation of the cells, the absorbance (optical density) of each cell suspension was measured in triplicate at 600 nm using an UV−vis spectrophotometer (Cary 3G, Varian). To study cell morphology and to quantitatively determine the number of chromosomes in individual cells, each cell suspension was imaged using dark-field optical and epi-fluorescence microscopy.

Single Live Cell Imaging. A total of 20 μL of the cell solution containing 10 μM EtBr and chloramphenicol (0, 6.25, 12.5, 25.0, 50.0, and 250 μg/mL) was added into a microchannel. The microchannel was constructed by sandwiching the solution between a microscope slide and a cover slip and then sealed with glue to prevent evaporation of the aqueous solution as described previously (*23*−*24*). We have successfully used this microchannel to overcome the rapid motion of tiny microbial cells in solution and to continuously monitor single bacterial cells in the microchannel for hours (*23*−*26*). In comparison with eukaryotic cells (average size of 10 μm), it is much more challenging to image single bacterial cells in suspension because tiny microbial cells (average size of 2 × 0.5 × 0.5 μm) can move much more rapidly in solution. Furthermore, only a single copy of the chromosome is present in a single bacterial cell, whereas there are multiple copies of chromosomes in eukaryotic cells. Thus, much more sensitive detection is needed to detect chromosomes in single microbial cells than in single eukaryotic cells. We have already used our single living cell microscopy to detect a single copy of chromosomes in single bacterial cells (*23*, *25*).

In this study, 10 representative locations in the microchannel were randomly chosen, and the cells in these locations were imaged using dark-field optical and epi-fluorescence microscopy. The dark-field optical and epi-fluorescence microscope was equipped with an oil dark-field condenser (Oil 1.43−1.20, Nikon), a 100× objective (Nikon Plan fluor 100× oil; iris; SL N.A. 0.5−1.3; W.D. 0.20 mm), a microscope illuminator (100 W halogen) for dark-field optical imaging, a super high-pressure mercury lamp (Nikon) for fluorescence imaging, and a CCD camera (Micromax, 5 MHz Interline, PID 1030 × 1300, Roper Scientific) for high-

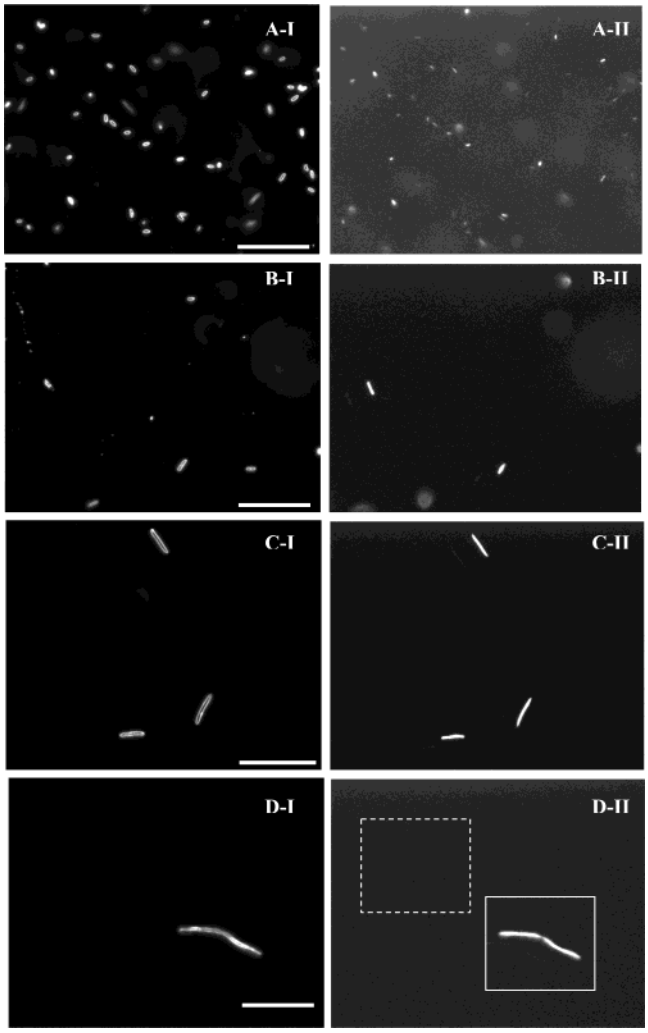

FIGURE 1: Representative full-frame (I) optical and (II) fluorescent images of the live cells (WT) acquired using a CCD camera through a dark-field microscope with CCD exposure time at 100 ms. All images were acquired from the cells in 10 μM EtBr solution containing (A) 0, 6.25, and 12.5 μg/mL; (B) 25.0 μg/mL; (C) 50.0 μg/mL; and (D) 250 μg/mL chloramphenicol, respectively. Scale bars are 20 μm. The intensity scale is 190−882 ADC.

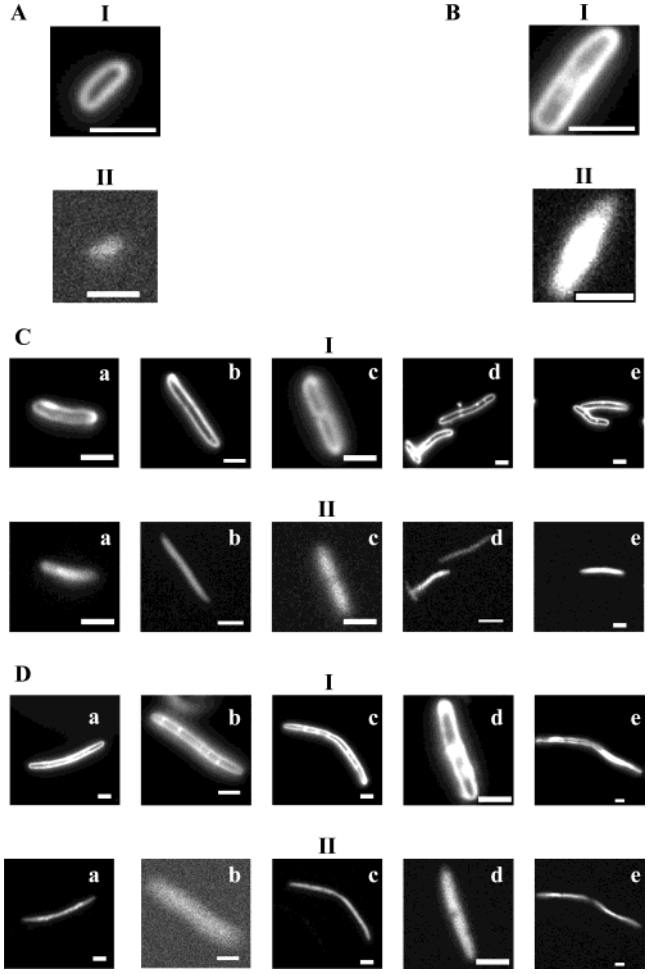

FIGURE 2: Representative dark-field optical (I) and fluorescent (II) images of the live cells (WT) in 10 μM EtBr solution containing (A) 0, 6.25, and 12.5 μg/mL; (B) 25.0 μg/mL; (C) 50.0 μg/mL; and (D) 250 μg/mL chloramphenicol, respectively. Images are selected from full-frame images similar to the ones shown in Figure 1. Scale bars are 2 μm. The intensity scale for (I) and (II) is 190−882 and 172−209 ADC, respectively.

speed and high-resolution cell imaging (*23*, *25*). The fluorescence images were acquired through a filter cube containing a band-pass excitation filter (488 ± 10 nm, Coherent), band-pass emission filter (600 ± 30 nm, Coherent), and a dichroic mirror (565 nm, Chroma Tech).

Data Analysis and Statistics. The full-frame CCD image (Figure 1) is able to simultaneously monitor ∼50 normal sized cells in the microchannel. Ten full-frame images were recorded for each experiment. For each concentration and each strain, four experiments were performed. Thus, 2000 cells of each strain were studied and analyzed. The length of the cells was directly measured using both Winview (Roper Scientific) and MetaMorph software (Universal Imagine). Each pixel of CCD represents a square with 0.067 μm edges, as calibrated by the microscope stage micrometer (0.1 mm per 50 divisions) via the 100× objective. The average length of normal sized cells is determined to be 1.73 ± 0.05 μm, whereas the average length of filamentous cells is 9.34 ± 0.83 μm, with a range from 6 to 25 μm (Figures 2−4). To determine the number of chromosomes in individual cells, we select an area (350 × 350 pixels) that contains an individual cell (solid-line square) and an equal sized area that contains no cells (solution only, dash-line square) in the same frame (Figure 1: D-II). We then analyze the integrated fluorescence intensity of each area and subtract the integrated intensity of the area (dash-line square) where no cell (solution only) was present from the integrated intensity of the area containing the cell (solid-line square). This subtraction is used to overcome possible dark noise of the CCD camera and photodecomposition of EtBr. It is also utilized to ensure that the fluorescence intensity reflects the number of chromosomes in an individual cell (Figure 3). The imaging station and software (Winview and MetaMorph) allow quantitative analysis of analog and digital counts (ADC) from each pixel. The ADC can be converted to a photoelectron count (10× for our CCD camera) that represents the digitized electrons accumulated in each pixel and hence reflecting the photons collected by the pixel during the exposure of the CCD camera. Thereby, ADC is an arbitrary unit for the relative quantitative measurement of intensity of specimens imaged by the CCD camera (*23*, *25*). Each optical and fluorescence image is presented using the

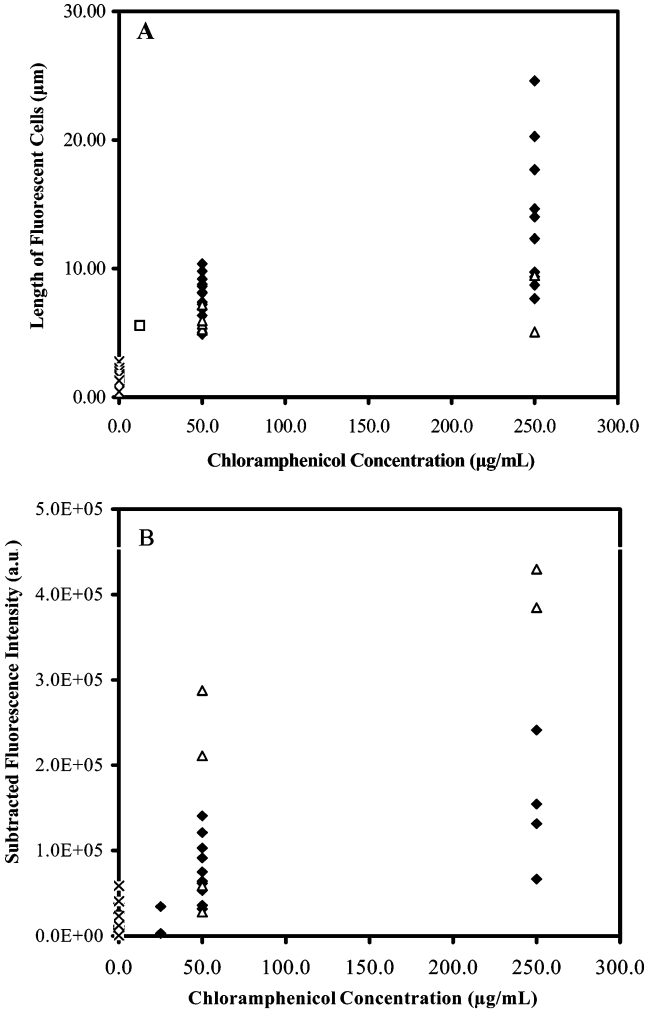

FIGURE 3: Plots of (A) optical length of fluorescent cells and (B) subtracted integrated fluorescent intensity of the cells versus chloramphenicol concentration: WT (◆), nalB-1 (△), ΔABM (□), and normal sized cells (×) (average length for all nonfilamentous cells), respectively.

same scale of ADC, 190−882 ADC and 170−209 ADC, respectively (Figures 5 and 6). Thus, the variation of the intensity in each image can be directly visualized, representing the contours of the distribution of chromosomes in the cells (Figures 5 and 6: II).

RESULTS AND DISCUSSION

Concentration Dependence. WT cells incubated in 10 μM EtBr and 0−250 μg/mL chloramphenicol were directly imaged using dark-field optical and fluorescence microscopy. Representative images of the cells from these solutions (Figures 1A,B and 2A,B) show that the morphology and length of the cells (2−3 μm) remain almost unchanged in 0, 6.25, 12.5, and 25.0 μg/mL chloramphenicol. In contrast, the filamentous WT cells 6−25 μm in length were observed in 50.0 and 250 μg/mL chloramphenicol (Figures 1C,D and 2C,D). Cell lengths increase notably as the chloramphenicol concentration increases (Figure 3A). Histograms of a length of ∼5000 cells in 0−250 μg/mL chloramphenicol (Figure 4) show that the normal sized cells are observed in 0, 6.25, 12.5, and 25.0 μg/mL chloramphenicol, and filamentous cells with a variety of lengths are observed in 50.0 and 250 μg/mL chloramphenicol. This result suggests that chloramphenicol induces the formation of filamentous WT cells and that the length of filamentous cells is related to the concentration of chloramphenicol.

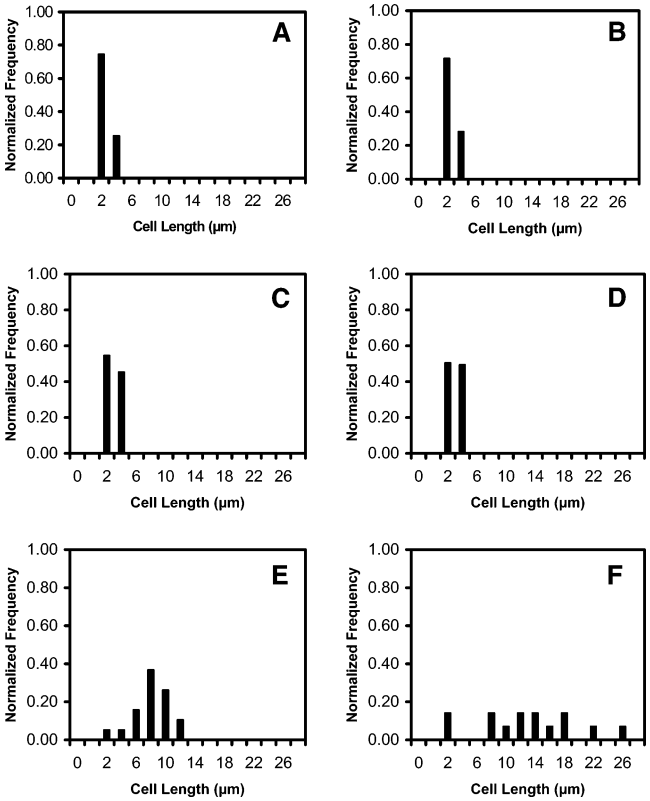

FIGURE 4: Histograms of the optical lengths of the live cells (WT) incubated with 10 μM EtBr solution containing (A) 0, (B) 6.25, (C) 12.5, (D) 25.0, (E) 50.0, and (F) 250 μg/mL chloramphenicol, respectively. Total numbers of ∼5000 cells are analyzed.

To investigate the number of chromosomes in individual cells, EtBr is used as a fluorescence probe. EtBr has been widely used as a fluorescence probe to study the uptake and extrusion mechanism in *P. aeruginosa* (*16*, *19*, *22*−*28*). It has been demonstrated that EtBr enters the live bacterial cells through passive diffusion and intercalates with DNA in the cells (*16*, *19*, *22*), leading to the 10-fold enhancement of fluorescence intensity. This feature allows us to directly observe and measure the replication and distribution of chromosomes in individual cells using fluorescence microscopy and spectroscopy. The minimum inhibitory concentration (MIC) of EtBr for all three strains of *P. aeruginosa* is higher than 1 mM (*19*, *26*). Thus, a low concentration EtBr (10 μM) does not significantly perturb cellular function and can be used as a fluorescence probe for live cell imaging (*23*−*26*). Our previous data have demonstrated that the accumulation of EtBr in WT cells remains unchanged after the cells have been incubated with 10 μM EtBr for 2 h (*23*−*25*). Therefore, the fluorescence intensity can be used to measure the number of chromosomes in cells that have been incubated with 10 μM EtBr for 2 h.

In dark-field optical microscopy, only scattered light from the specimen captured by the objective lens creates images. Thus, the images emerge bright against a dark background (*33*). The specimen that scatters light most efficiently generates the brightest image. This unique feature has proven dark-field microscopy to be well-suited for the imaging of species with small sizes, such as live bacterial cells with an

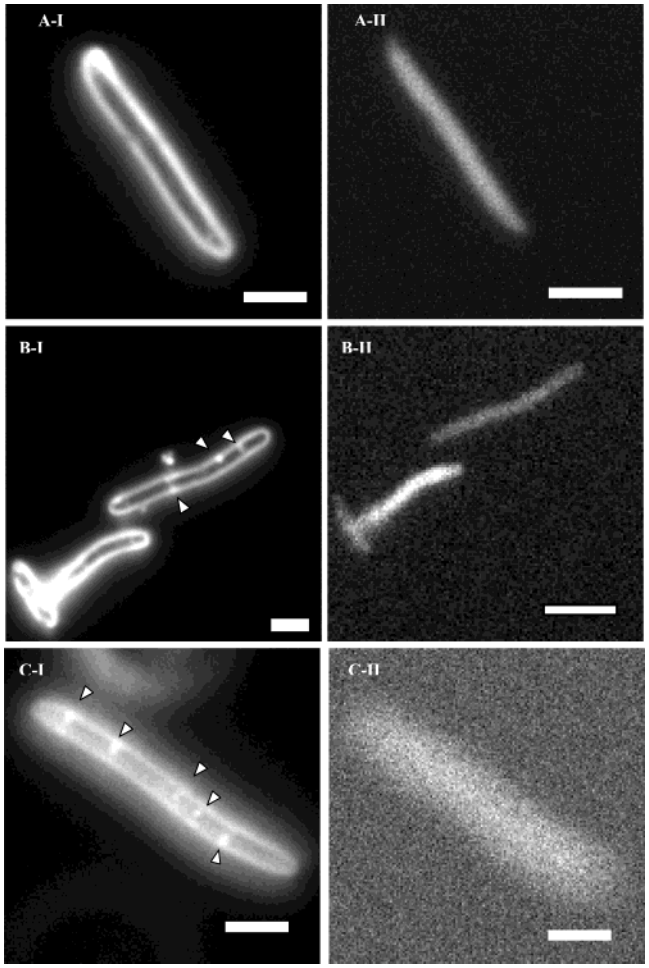

FIGURE 5: Representative dark-field optical (I) and fluorescent (II) images of the live cells (WT) in 10 μM EtBr solution containing (A and B) 50.0 μg/mL and (C) 250 μg/mL chloramphenicol, respectively. Images are selected from full-frame images similar to the ones shown in Figure 1. Scale bars are 2 μm. The intensity scale for (I) and (II) is 190−882 and 172−209 ADC, respectively. The arrows point out to the locations of septa.

average size of 2 × 0.5 × 0.5 mm (*33*). The cytoplasmic space is surrounded by the periplasmic space. Hence, the light from the microscope illuminator needs to penetrate the periplasmic space to reach the cytoplasmic space. The periplasmic space absorbs and scatters the light. As a result, the intensity of the illumination was weaker in the cytoplasmic space than in the periplasmic space. For this reason, optical images of single cells acquired by dark-field microscopy (Figures 5 and 6: I) clearly distinguish the contours of the periplasmic space (bright) and cytoplasmic space (dim). In contrast, the fluorescent images (Figures 5 and 6: II) display a bright cytoplasmic space and a dim periplasmic space. Therefore, the fluorescence of EtBr is primarily observed in the cytoplasmic space where DNA and RNA are present. This result demonstrates that the fluorescence intensity of EtBr in cells represents the quantity of DNA and RNA, and the fluorescence intensity can be used to quantitatively measure the amount of replicated chromosomes in cells because the amount of RNA remains relatively small in comparison with large chromosomes.

As the cell length increases along with the chloramphenicol concentration, the length of fluorescent chromosomes (Figures 5 and 6: II) and the fluorescence intensity of the

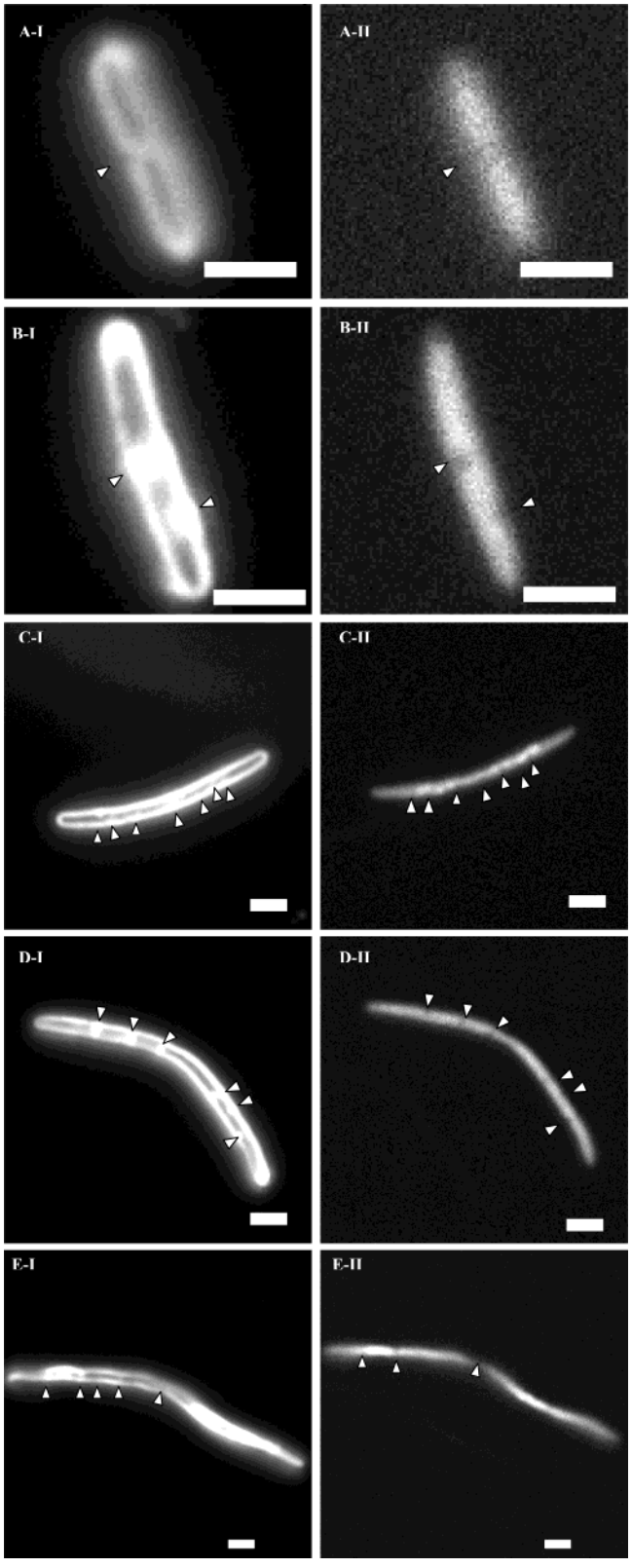

FIGURE 6: Representative dark-field optical (I) and fluorescent (II) images of the cells (WT) in 10 μM EtBr solution containing (A) 50.0 μg/mL and (B−E) 250 μg/mL chloramphenicol, respectively. Images are selected from full-frame images similar to the ones shown in Figure 1. Scale bars are 2 μm. The intensity scale for (I) and (II) is 190−882 and 172−209 ADC, respectively. The arrows point out to the locations of septa.

individual cells also increases (Figure 3B). This suggests that the chromosomes are replicated in individual filamentous cells and that multiple copies of chromosomes are present

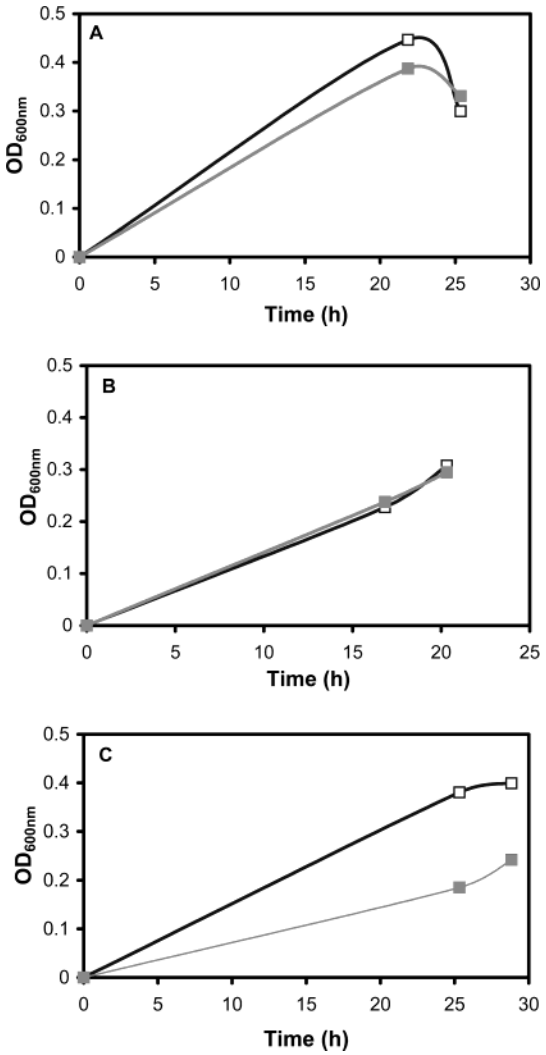

FIGURE 7: Representative cell growth curves from the preculture solution of (A) WT, (B) nalB-1, and (C) ΔABM. (■) represents the cells that have been incubated with 100 μM EtBr and 25 μg/mL chloramphenicol for 2 h, and (□) represents the cells that have not been incubated with EtBr and chloramphenicol.

in these cells. The optical and fluorescence images of the cells in Figures 5 and 6 show that each filamentous cell consists of discrete entities (undivided cells) and that each entity appears to contain one copy of the bacterial chromosome. This observation suggests a mechanism whereby filamentous bacteria successfully and rapidly divide and recolonize after the removal of antibiotics (*4*).

Chloramphenicol is neither a β-lactam nor an aminoglycoside antibiotic. Its primary target is ribosomal peptidyl transferase, where it acts competitively to inhibit normal substrate binding (*29*). Chloramphenicol has also been known as a bacteriostatic agent that inhibits bacterial growth by targeting ribosomal peptidyl transferase and inhibiting protein synthesis (*29*). As the chloramphenicol concentration decreases, the cells resume the growth and division (*29*). To study the viability of the cells, we measured the cell growth curves (Figure 7). We took 20 μL of the cultured cell solutions that had been incubated with 25 μg/mL chloramphenicol and 100 μM EtBr for 2 h and added it into 2 mL of L-broth medium to prepare a highly diluted cell culture suspension. The scattering of cells at 600 nm ($OD_{600\ nm}$) is typically used to determine the concentration of bacterial cells. Thus, the cell growth curves are measured by the monitoring of cell concentration with time using absorbance at 600 nm ($OD_{600\ nm}$). The cells that had been incubated with 25 μg/mL chloramphenicol and 100 μM EtBr for 2 h have similar growth curves to those that had not been incubated with EtBr and chloramphenicol (Figure 7). It is interesting to note that the cell growth curves show mutant dependence (Figure 7). The mutant that overexpresses MexAB-OprM (nalB-1) shows the highest resistance to EtBr and chloramphenicol. Thus, the growth curve of nalB-1 cells that had been incubated with EtBr and chloramphenicol is almost identical to the growth curve of the cells that were grown in the absence of EtBr and chloramphenicol. In contrast, the mutant deficient of MexAB-OprM (ΔABM) shows the lowest resistance to EtBr and chloramphenicol. Thus, ΔABM cells that had been incubated with EtBr and chloramphenicol grew much more slowly than the cells that were grown in the absence of EtBr and chloramphenicol. To investigate cellular morphology and cell growth at single cell resolution, optical images of the cells from these cell suspensions were acquired over time, showing that a few cells were introduced into the culture medium initially. After incubation in the shaker at 120 rpm and 37 °C, these cells grew, divided, and generated normal sized cells, demonstrating that the cells that had been incubated with 25 μg/mL chloramphenicol and EtBr for 2 h in Figure 1 are still alive.

It is noteworthy that the distribution of cell lengths and number of chromosomes in individual cells becomes widely varied as the chloramphenicol concentration increases (Figures 2−4). As the chloramphenicol concentration increases, a few of the cells remain in the normal sized range (2−3 μm), while other cells increase in length and generate filaments of various sizes (Figures 2−4). This suggests that individual cells have different responses to chloramphenicol, further emphasizing the importance of studying filamentation at single cell resolution. To determine whether EtBr affects the filamentation, similar experiments were carried out in the absence of EtBr and in the presence of Hoechst 33258 (a fluorescence probe that specifically binds with DNA only) (*34*). Similar histograms are generated from the experiments (Figure 1S, Supporting Information). These data demonstrate that the presence of 10 μM EtBr has little effect on the cell filamentation.

Morphologies and Chromosomes of Single Filamentous Live Cells. Many single cells were monitored simultaneously (Figure 1) and analyzed quantitatively in each frame (Figures 3 and 4). Representative cells selected from the full-frame images in Figure 1 are shown in Figures 2, 5, and 6, presenting the morphologies of individual cells in detail. Some cells retain normal morphology, exhibiting the same lengths as normal cells as the chloramphenicol concentration increases (Figure 2C: a). In contrast, other cells increase their lengths and turn to filaments with aseptate (Figure 5A) or partially septate and aseptate (Figures 5B,C and 6) forms.

Fluorescence images in Figure 5-II show that the chromosomes in some individual cells are unsegregated. These chromosomes are observed as a continuous filament in the cells. In contrast, fluorescent images in Figure 6 show that chromosomes in some cells are constricted by intact septa. The fluorescent images of these individual cells (Figure 6) show the highest intensity in the center of discrete entities (undivided cells) and the weakest intensity at the septa. The

Table 1: Summary of Occurrences of Filamentation from All Experiments

strains	chloramphenicol concn (μg/mL)	experiments	occurrence[a]	frequency[b] (%)
WT	0	4	0	0
	6.25	4	0	0
	12.5	4	0	0
	25.0	4	0	0
	50.0	4	4	100
	250.0	4	2	50
nalB-1	0	4	0	0
	6.25	4	0	0
	12.5	4	1	25
	25.0	4	2	50
	50.0	4	4	100
	250.0	4	4	100
ΔABM	0	4	0	0
	6.25	4	1	25
	12.5	4	1	25
	25.0	4	0	0
	50.0	4	0	0
	250.0	4	0	0

[a] Represent the number of experiments that resulted in filamentous cells. [b] Represent the percentage of experiments that resulted in filamentous cells.

pattern of fluorescence in the cells reveals the traces of attempted chromosomal segregation in live cells, suggesting that the chromosomes struggled to segregate but failed in completion of the entire segregation. The unsuccessful segregation of multiple copies of chromosomes could have led to the failure of cell division. In this study, both septate and aseptate filaments (elongated rods) are observed. However, other morphological forms (e.g., spheroplasts) are not observed. Previous reports have indicated that several antibiotics (e.g., carbapenems, imipenem, panipenem, and biapenem) bind primarily to PBP-2 of *P. aeruginosa*, leading to the formation of spheroplasts (*2*−*3*). In contrast, ceftazidime binds primarily with PBP-3 of *P. aeruginosa*, which leads to filamentation (*4*). Chemically, it is unlikely that chloramphenicol has a specific affinity with PBP. One plausible explanation is that chloramphenicol induces filamentation by targeting ribosomal peptidyl transferase and hence inhibiting the expression of PBP.

Mutant Dependence. To study whether the filamentation depends on the expression level of MexAB-OprM (extrusion pump), strains of WT, nalB-1, and ΔABM were incubated with 0−250 μg/mL chloramphenicol. Four experiments were performed on each cell type at each chloramphenicol concentration. Occurrences of filamentation in three strains of *P. aeruginosa* are summarized in Table 1, showing that filamentation is not observed in the absence of chloramphenicol. Filamentous WT cells are observed in 50 and 250 μg/mL chloramphenicol, with the highest occurrences (100%) at 50 μg/mL (2 × MIC). Unlike WT, filamentous nalB-1 cells are observed through the wide range of chloramphenicol concentrations (12.5−250 μg/mL), with the highest occurrences (100%) at 50 and 250 μg/mL. In contrast, filamentous ΔABM cells are observed in a much lower chloramphenicol concentration of 6.25 and 12.5 μg/mL and show lower occurrences (25%).

The mutants differ only in the level of expression of MexAB-OprM. The mutant (ΔABM) that does not express MexAB-OprM is unable to extrude cytotoxic substances (chloramphenicol) out of cells as effectively as WT. Hence, ΔABM accumulates chloramphenicol much more rapidly. In contrast, the mutant (nalB-1) with the high expression level of MexAB-OprM is able to extrude chloramphenicol out of cells much more effectively than WT, leading to the slower accumulation of chloramphenicol in the cells. Because of the different expression levels of MexAB−OprM in these three strains, MIC of chloramphenicol for ΔABM, WT, and nalB-1 is 12.5, 25 and 50 μg/mL, respectively (*21*, *26*, *27*). This has a marked effect on cell viability (Figures 3,7). Typically, only a few ΔABM cells were observed in chloramphenicol concentrations above 12.5 μg/mL. Thus, there is insufficient number of filamentous ΔABM cells in all selected chloramphenicol concentrations (0, 6.25, 12.5, 25.0, 50.0, and 250 μg/mL) (Figure 3).

For WT, filamentation appears highly associated with MIC. The filamentous WT cells are observed only above the MIC at 50 μg/mL (2 × MIC) and 250 μg/mL (10 × MIC), which agrees well with previous reports using other types of antibiotics (*2*, *4*, *5*, *7*, *35*). Unlike WT, filamentation in ΔABM is not observed beyond its MIC (12.5 μg/mL), whereas filamentation in nalB-1 is observed both below and beyond its MIC (50 μg/mL). These findings are significantly different from the previously reported data (*2*, *4*, *5*, *7*, *35*), which shows that filamentation typically starting at 0.5 × MIC to well over 100 × MIC. This new finding appears attributable to the use of single live cell imaging. This approach allows us to directly monitor many single live cells simultaneously in solution at single cell resolution.

CONCLUSION

In this study, we present a new platform for the quantitative study of chromosomes in filamentous Gram-negative bacteria (*P. aeruginosa*) induced by chloramphenicol using single live cell imaging. We find that chloramphenicol can induce the formation of filamentous cells, which contain multicopies of unsegregated chromosomes, leading to the unsuccessful division of elongated cells and the formation of bacterial filaments. The study of filamentation at single live cell resolution offers new insights into filamentation mechanisms. For example, the quantity of chromosomes and the length of individual filamentous cells (WT) become highly varied as the chloramphenicol concentration increases, suggesting that individual cells differ their response to chloramphenicol. Furthermore, this study indicates that filamentation occurrences depend on expression levels of an efflux pump (MexAB-OprM), showing the important role of the extrusion pump in bacterial filamentation. Moreover, this study opens up the new possibility of real-time monitoring of modes of actions of antibiotics in live cells with both temporal and spatial resolution. One can now use this new approach to further study the function of antimicrobial agents on cell growth and division, as well as to carry out biochemical and biophysical measurements in real time at single live cell and single chromosome levels.

ACKNOWLEDGMENT

We thank Taiji Nakae (Tokai University School of Medicine, Japan) and Hiroshi Yoneyama (Tohoku University, Japan) for three strains of *P. aeruginosa*.

SUPPORTING INFORMATION AVAILABLE

Histograms of the optical lengths of live cells. This material is available free of charge via the Internet at http://pubs.acs.org.

REFERENCES

1. Tomasz, A. (1986) *Rev. Infect. Dis. 8(Suppl 3)*, S260−S278.
2. Horii, T., Kobayashi, M., Sato, K., Ichiyama, S., and Ohta, M. (1998) *J. Antimicrob. Chemother. 41*, 435−442.
3. Gould, I. M., and MacKenzie, F. (1997) *J. Antimicrob. Chemother. 40*, 495−499.
4. Hanberger, H., Nilsson, L. E., Nilsson, M., and Maller, R. (1991) *Eur. J. Clin. Microbiol. Infect. Dis. 10*, 927−934.
5. Horii, T., Ichiyama, S., Ohta, M., and Kobayashi, M. (1999) *J. Med. Microbiol. 48*, 309−315.
6. Rajyaguru, J. M., Torres, D. S., Abel, E., Richardson, M. C., and Muszynski, M. J. (1998) *J. Antimicrob. Chemother. 41*, 557−561.
7. Nakao, M., Kondo, M., and Imada, A. (1986) *J. Antimicrob. Chemother. 17*, 433−439.
8. Nakao, M., Noji, Y., Iwahi, T., and Yamazaki, T. (1992) *J. Antimicrob. Chemother. 29*, 509−518.
9. Greenwood, D. (1997) *J. Antimicrob. Chemother. 40*, 499−501.
10. Turcotte, A., Simard, M., Morin, N. J., Beauchamp, D., and Bergeron, M. G. (1997) *Antimicrob. Agents Chemother. 41*, 401−409.
11. Bucklin, S. E., Fujihara, Y., Leeson, M. C., and Morrison, D. (1994) *Eur. J. Clin. Microbiol. Infect. Dis. 13(Suppl 1)*, S43−S51.
12. Aonuma, S., Ariji, F., Oizumi, K., and Konno, K. (1986) *Tohoku J. Exp. Med. 150*, 69−75.
13. Van Helvoort, J. M., Huls, P. G., Vischer, N. O., and Woldringh, C. L. (1998) *Microbiology. 144*, 1309−1317, and references therein.
14. Poole, K. (2001) *J. Mol. Microbiol. Biotechnol. 3*(2), 255−264.
15. Nakae, T. (1997) *Microbiologia 13(3)*, 273−284, and references therein.
16. For review: Ryan, B. M., Dougherty, T. J., Beaulieu, D., Chuang, J., Dougherty, B. A., and Barrett, J. F. (2001) *Expert Opin. Investig. Drugs 10*(8), 1409−1422, and references therein.
17. Ma, D., Cook, D. N., Hearst, J. E., and Nikaido, H. (1994) *Trends Microbiol. 2*(12), 489−493.
18. Maseda, H., Yoneyama, H., and Nakae, T. (2000) *Antimicrob. Agents Chemother. 44(3)*, 658−664.
19. Ocaktan, A., Yoneyama, H., and Nakae, T. (1997) *J. Biol. Chem. 272*, 21964−21969.
20. Saito, K., Yoneyama, H., and Nakae, T. (1999) *FEMS Microbiol. Lett. 179*(1), 67−72.
21. Yoneyama, H., Ocaktan, A., Tsuda, M., and Nakae, T. (1997) *Biochem. Biophys. Res. Commun. 233*, 611−618.
22. Morgan, A. R., Lee, J. S., Pulleyblank, D. E., Murray, N. L., and Evans, D. H. (1979) *Nucleic Acids Res. 7*(3), 547−569, and references therein.
23. Kyriacou, S., Nowak, M., Brownlow, W., and Xu, X.-H. N. (2002)- *J. Biomed. Opt. 7*, 576−586.
24. Xu, X.-H. N., Brownlow, W., Huang, S., and Chen, J. (2003) *Biochem. Biophys. Res. Commun. 305*, 79−86.
25. Xu, X.-H. N., Wan, Q., Kyriacou, S., Brownlow, W., and Nowak, M. (2003) *Biochem. Biophys. Res. Commun. 305*, 941−949.
26. Kyriacou, S. V. (2003) Real-time study of multidrug resistance mechanism in *Pseudomonas aeruginosa* using nanoparticle optics and single live cell imaging, Master Thesis, Old Dominion University, Norfolk, VA.
27. Xu, X.-H. N., Kyriacou, S., Brownlow, W., Wan, Q., and Viola, J., submitted.
28. Kyriacou, S. V., Brownlow, W., and Xu, X.-H. N. (2004) *Biochemistry 43*(2), in press.
29. Greenwood, D. (1997) Modes of action in antibiotic and chemotherapy, in *Antibiotic and Chemotherapy: Anti-infective Agents and Their Use in Therapy* (O'Grady, F., Lambert, H. P., Finch, R. G., and Greenwood, D., Eds.) 7th ed., pp 10−21, Churchill Livingstone, New York.
30. National Committee for Clinical Laboratory Standards (2000) *Methods for Dilution of Antimicrobial Susceptibility Tests for Bacteria that Grow Aerobically*, 5th ed., Approved Standard NCCLS Document M7-A5, Vol. 20, No. 2. p 44, NCCLS, Wayne, PA.
31. Fowler, C. E., Soothill, J. S., and Oakes, L. (1997) *J. Antimicrob. Chemother. 40*, 877−879.
32. Li, X. Z., Livermore, D. M., and Nikaido, H. (1994) *Antimicrob. Agents Chemother. 38*, 1732−1741.
33. Freifelder, D. (1982) *Physical Biochemistry*, pp 51−52, Freeman, New York.
34. Haugland, R. P. (2002) *Handbook of Fluorescent Probes and Research Products*, 9th ed., pp 278−281, Molecular Probes, Inc., Eugene, OR.
35. Trautmann, M., Heinemann, M., Zick, R., Möricke, A., Seidelmann, M., and Berger, D. (1998) *Eur. Clin. Microbiol. Infect. Dis. 17*, 754−760.

BI035341E